

## High efficient photodegradation of organic dyes by TiO<sub>2</sub>/graphene composite under visible light radiation

Guoling Li<sup>a</sup>, Jianzeng Liu<sup>a</sup>, Ting Zhou<sup>a</sup>, Shirong Li<sup>b</sup>, Yunshan Bai<sup>a,\*</sup>, Huanhuan Liu<sup>b,\*</sup>

<sup>a</sup>School of Chemistry and Chemical Engineering, Shaanxi Normal University, No. 620, West Chang'an Avenue, Chang'an District, Xi'an, Shaanxi 710119, China, emails: baiys@snnu.edu.cn (Y. Bai), 792239171@qq.com (G. Li), 862882513@qq.com (J. Liu), 735055591@qq.com (T. Zhou)

<sup>b</sup>Basic Experimental Teaching Center, Shaanxi Normal University, No. 199, South Chang'an Road, Yanta District, Xi'an, Shaanxi, 710062, China, emails: hhlui@snnu.edu.cn (H. Liu), lishirong@snnu.edu.cn (S. Li)

Received 17 October 2019; Accepted 14 October 2020

### ABSTRACT

An efficient visible light-responsive TiO<sub>2</sub>/graphene composite was synthesized easily by grinding. The structure and morphology of the composite were characterized by powder X-ray diffraction, Raman spectroscopy, ultra-high-resolution transmission electron microscopy, and field emission scanning electron microscopy. The photocatalytic characteristics were studied by degrading methylene blue under different conditions such as pH, catalyst dosage, different wt.% ratios of TiO<sub>2</sub>/graphene composites, irradiation time, and initial concentration of methylene blue. The results showed that the TiO<sub>2</sub>/2.0% graphene possessed much higher photocatalytic activities under visible light than pure TiO<sub>2</sub>, displayed high photochemical stability under repeated irradiation, and can also effectively and selectively degraded a mixture of methyl orange and methylene blue. The degradation of methylene blue followed the pseudo-first-order kinetics of Langmuir–Hinshelwood model. In addition, the possible mechanism of photocatalytic degradation process was proposed.

*Keywords:* TiO<sub>2</sub>; Graphene; Methylene blue; Photocatalysis; Mechanism

### 1. Introduction

TiO<sub>2</sub> is one of the most popular photocatalysts in the degradation and oxidation of hazardous materials to non-toxic compound [1]. It has been attracted a great deal of research interest due to the rapid development of dyestuff industry [2,3]. Unfortunately, the quantum efficiency of photocatalytic reaction is low because of the rapid recombination of electrons and holes [4,5]. Moreover, the pure TiO<sub>2</sub> as photocatalyst has been restricted to the ultraviolet environment owing to its wide band gap (anatase,  $E_g = 3.2$  eV) [6]. At present, the focal points on TiO<sub>2</sub> photocatalytic materials are to improve the visible light response and reduce the recombination probability of excited electron–hole pair [7,8].

In recent years, graphene (GR) has been widely used in various fields because of its large specific surface area, fast electron transmission, and high mechanical strength. Due to the conjugate structure of GR, it is favorable for charge separation in photocatalytic process [7]. The complexes of graphene oxide (GO)/TiO<sub>2</sub> and reduced graphene oxide (RGO)/TiO<sub>2</sub> have been reported [8–10]. However, most methods for preparing these complexes are high temperature processes, resulting in expensive preparation cost, high energy consumption [7–9,11]. Furthermore, they were limited to carry out in a small amount. Herein, an efficient visible light-responsive TiO<sub>2</sub>/GR composite was synthesized simply by grinding on large-scale and characterized

\* Corresponding authors.

by different techniques. The photocatalytic characteristics were investigated by degrading methylene blue (MB) and a mixture of methyl orange (MO) and methylene blue under different conditions such as pH, catalyst amount, different ratios of TiO<sub>2</sub>/GR, irradiation time, and initial concentration of the MB dye. Moreover, the kinetics of degradation process were also discussed.

## 2. Experimental

### 2.1. Materials and reagents

Methane (99.99%) and argon (99.99%) were purchased from Xi'an Tenglong Chemical Co., Ltd., in Xijing 3, Dianzi West Street, Yanta District, Xi'an, China. Titanium dioxide was purchased from Tianjin Yaohua Chemical Reagent Co., Ltd., in North side of Xuelian bridge, Jinbin Avenue, Dongli District, Tianjin, China. Sodium hydroxide, hydrochloric acid, methylene blue, and methyl orange in analytical purity were purchased from China Pharmaceutical Group Chemical Reagent Co., Ltd., in East Street, Beilin District, Xi'an, China.

### 2.2. Preparation of graphene

Graphene was synthesized by the chemical vaporous deposition (CVD) method. The temperature was chosen 950°C with a temperature ramp-up rate of 20°C/min. Methane gas was used as a carbon precursor in the mixture of Ar and CH<sub>4</sub> in the gas flow ratio of 1:2 for graphene deposition.

### 2.3. Preparation of TiO<sub>2</sub>/GR composite

GR and TiO<sub>2</sub> were mixed in a certain proportion and ground for 3 h to produce the composite. The GR doping amounts were 0.5%, 1.0%, 1.5%, 2.0%, 2.2%, and 2.5%, respectively.

### 2.4. Characterization

The surface morphology and structure of TiO<sub>2</sub>/GR composites were analyzed using field emission scanning electron microscopy (SEM, SU8220, Hitachi) and ultra-high-resolution transmission electron microscopy (HR-TEM, JEM-2100). The Raman spectroscopy (Raman Spectrometer, in Via Reflex Britain) were characterized under 532 nm. X-ray diffraction (XRD, Bruker, Germany) patterns were carried out by using a D8 advance X-ray diffractometer with Cu K<sub>α</sub> radiation. The UV-vis diffuse reflectance spectra (UV-vis/DRS) in the range 200–800 nm were recorded on a UV-vis-NIR spectrophotometer (Perkin-Elmer Inc., Lambda 1050) equipped with an integrating sphere using BaSO<sub>4</sub> as a reference.

### 2.5. Photocatalytic activity testing

The photocatalytic activity of composites were estimated by degrading MB in a self-assembled apparatus with a homemade photoreactor which was equipped with 100 W tungsten lamp (Basda lighting appliances Co., Ltd.) as the radiation source. It was placed 1 cm above the solution. The visible-light ( $\lambda \geq 400$  nm) was obtained by the filter with a cut-off wavelength of 400 nm. The initial concentrations of the MB dye solution were 0.0550, 0.0749, 0.0949, 0.1150, and 0.1350 mmol/L, respectively. The reaction took place at

room temperature. The pH of the solution was adjusted by 0.5 mol/L HCl and 2.5 mol/L NaOH. All of solid particles in liquids were completely removed before measuring the UV-vis absorption of solutions. Four milliliters of liquid was sucked out with a pipette and monitored with a UV spectrometer (UVT6, Beijing Purkinje General Instrument Co., Ltd., China) from the absorbance at the wavelength of the main absorption peak (664 nm). The intensity of the absorption peak of the MB dye was referred to as a measure of the residual MB dye concentration ( $c$ ).

The photocatalytic degradation efficiency ( $D\%$ ) of composites were calculated using Eq. (1) [12]:

$$D\% = \frac{A_0 - A_t}{A_0} \times 100\% = \frac{c_0 - c_t}{c_0} \times 100\% \quad (1)$$

where  $A_0$ ,  $A_t$  represent the absorbency of the MB dye in the photocatalytic reaction solution before and after irradiation,  $c_0$  and  $c_t$  (mmol/L) are the concentrations of the MB dye at an initial time and time  $t$  (min).

### 2.6. Recycling studies

In order to evaluate the stability and reusability of the TiO<sub>2</sub>/GR composites, a recycled photoactivity was carried out as follows. Typically, after photocatalytic reaction for 60 min under visible light, the composite was separated from the reaction solution, washed with anhydrous ethanol, and dried in an oven. Then it mixed with the fresh MB solution to perform the second run photoactivity testing. The recycled photoactivities were done for five times.

### 2.7. Adsorption and photocatalytic degradation kinetics

Fifty milligrams of the TiO<sub>2</sub>/GR composite was added into 20 mL MB solution with different initial concentrations and pH 12. Then, the MB solution was stirred magnetically and performed photodegradation reaction. Five parallel experiments were conducted for each factor for different periods of time (10–60 min).

The photocatalytic degradation rate of the MB dye can be described follow a Langmuir–Hinshelwood apparent first-order-kinetics model, described by Eqs. (2) and (3) [13]:

$$r = \frac{dc}{dt} = -kc \quad (2)$$

where  $r$  (mg/L/min) is the degradation rate of the reactant,  $k$  (1/min) is the reaction rate constant,  $t$  (min) is the visible light irradiation time and  $c$  (mmol/L) is the concentration of the dye at time  $t$ . When integrating Eq. (2) with the limit of  $c = c_0$  at  $t = 0$ , Eq. (2) can be simplified to an apparent first-order model [14]:

$$\ln\left(\frac{c_0}{c_t}\right) = k_a t \quad (3)$$

where  $c_0$  and  $c_t$  are the concentrations of the dye at an initial time and time  $t$ ,  $k_a$  is the apparent first-order rate constant of the photocatalytic degradation reaction.

### 3. Results and discussion

#### 3.1. Structural characterization

##### 3.1.1. X-ray diffraction

The GR, TiO<sub>2</sub>, and TiO<sub>2</sub>/GR composites with different contents of GR were characterized by XRD, as shown in Fig. 1a. The diffraction peaks for GR at 2θ = 26.5° (*d*-spacing = 0.34 nm) and 42.5° corresponded to the graphite crystallinity (002) and (100) [15], respectively. The position of the main peak of as-prepared graphene at 2θ = 25.8° (002, *d* = 0.35 nm) was observed, indicating the two-dimensional ordering of GR [16]. The characteristic peaks can be observed in different diffraction patterns at 25.3°, 36.9°, 37.8°, 38.6°, 48.0°, 53.9°, 55.1°, 62.7°, 68.8°, 70.3°, and 76.0°, which correspond to the (101), (103), (004), (112), (200), (105), (211), (204), (116), (220), and (301) crystal planes of TiO<sub>2</sub> anatase (JCPDS # 21-1272), respectively [17,18]. It was obviously displayed that the XRD patterns of the TiO<sub>2</sub>/GR composites with different contents of GR were very similar and no diffraction peaks of GR because the diffraction peak of GR located at 25.8° was masked by the strong and sharp (101) diffraction peak of anatase phase TiO<sub>2</sub> [19,20]. Compared with the pure TiO<sub>2</sub>, the characteristic diffraction peaks of anatase phase TiO<sub>2</sub> in the composites were strengthened. It was indicated that the crystallinity of anatase titanium dioxide was increased [17,21]. In addition, the crystal size

of titanium dioxide before and after doping graphene were calculated by the Debye–Scherrer equation formula as shown in Table 1. It was demonstrated that after graphene doping, the grain size of titanium dioxide becomes larger, which was consistent with the change of XRD diffraction peak intensity. All the above results indicated anatase TiO<sub>2</sub> had been loaded onto GR successfully.

##### 3.1.2. Raman spectra

To further confirm the simultaneous presence of TiO<sub>2</sub> and GR in the composites, the samples were investigated by using Raman spectroscopy (Fig. 1b). For TiO<sub>2</sub>, there were the four typical peaks at approximately 141, 395, 516, and 635 cm<sup>-1</sup> corresponding to E<sub>1g</sub>, B<sub>1g</sub>, A<sub>1g</sub> + B<sub>1g</sub>, and E<sub>2g</sub> modes, respectively, which were similar to the reported values for anatase TiO<sub>2</sub> [22]. For GR, the three characteristic peaks which were the D band at 1,354 cm<sup>-1</sup>, the G band at 1,598 cm<sup>-1</sup>, and the 2D band at 2,750 cm<sup>-1</sup> appeared in the Raman spectroscopy. They were consistent with the literature values [23,24]. The D band intensity provided an evidence of the presence of defects by ring vibrational mode of sp<sup>2</sup> hybridized carbon atoms, which was attributed to the A<sub>1g</sub> vibration mode of nanocrystalline graphite [25]. G band intensities of carbon materials were associated with the graphite lattice, representing the stretching of sp<sup>2</sup> type C=C bond in hexagonal ring structure in graphite lattice, which can be assigned to the E<sub>2g</sub> vibration mode [26,27]. Another 2D peak was ascribed to the vibrational mode of two photon lattices [28]. For the TiO<sub>2</sub>/GR composites, the four peaks of anatase TiO<sub>2</sub> still existed. It can be seen from the Raman spectra of 1,000–3,200 cm<sup>-1</sup> that the typical Raman peaks at 1,342 (D band), 1,594 (G band), and 2,740 cm<sup>-1</sup> (2D band (insert of Fig. 1b) were similar with the spectrogram of graphene. Compared to the pure graphene, the D peak of the composites shifted to high wave numbers by increasing the content of GR. Meanwhile, the G peaks of the composites also shift about 20 cm<sup>-1</sup> to high wave number, indicating the strong interaction of GR with TiO<sub>2</sub>. The intensity ratio of the D to G band (*I<sub>D</sub>/I<sub>G</sub>*) has been used to indicate the presence of defects in the structure of GR [29]. The *I<sub>D</sub>/I<sub>G</sub>* ratios for the GR, TiO<sub>2</sub>/0.5%GR, TiO<sub>2</sub>/1.0%GR, TiO<sub>2</sub>/1.5%GR, and TiO<sub>2</sub>/2.0%GR samples were 1.170, 1.065, 1.104, 1.104, and 1.001, respectively. The above results illustrated that more sp<sup>2</sup> domains have been formed in TiO<sub>2</sub>/GR composites. In addition, the sp<sup>2</sup> hybridization of carbon atoms has the lone pair electrons, which can form large

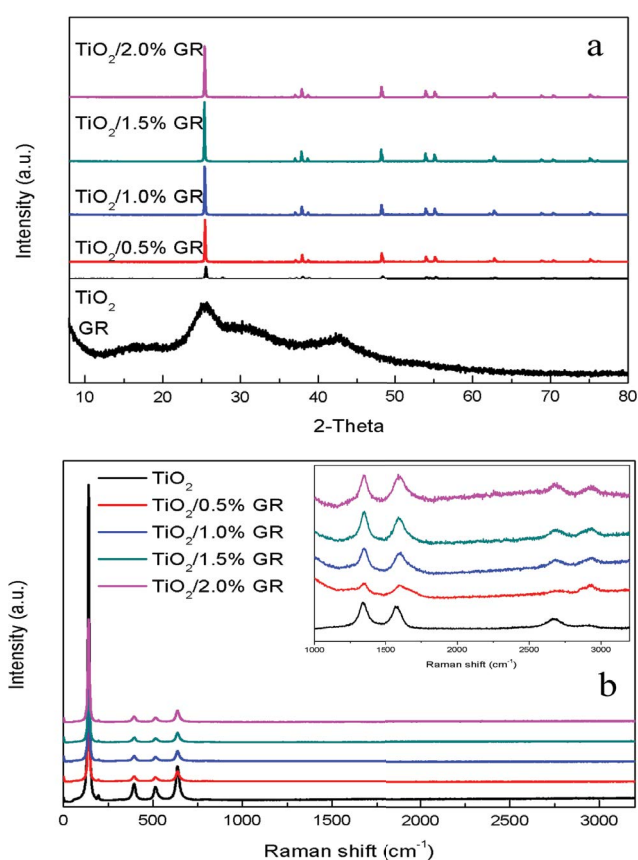


Fig. 1. (a) XRD patterns, (b) Raman spectra of GR, TiO<sub>2</sub>, and TiO<sub>2</sub>/GR with different contents of GR.

Table 1  
Lattice size of TiO<sub>2</sub> and TiO<sub>2</sub>-GC

Sample	X-ray diffraction angle (°)	Half peak width (rad)	Lattice size (nm)
TiO <sub>2</sub>	12.73	0.0028	49.20
TiO <sub>2</sub> /0.5GR	12.71	0.0018	78.68
TiO <sub>2</sub> /1.0GR	12.70	0.0018	77.69
TiO <sub>2</sub> /1.5GR	12.68	0.0016	85.94
TiO <sub>2</sub> /2.0GR	12.70	0.0018	77.69

the conjugative  $\pi$  system with other  $sp^2$  hybridization of carbon atoms. Thus, they can act as the rapid conduction electrons in the composites [30,31].

### 3.1.3. TEM and SEM

The morphologies of  $TiO_2$ , GR, and  $TiO_2/2.0\%GR$  composite were characterized by SEM and TEM, as shown in Fig. 2. For GR, there were flake-like shapes with lamella (Fig. 2a). While the image of pure  $TiO_2$  exhibited highly uniform nanocrystal structure (Fig. 2b). These two different morphologies can be clearly observed from the images of the composite (Fig. 2c). From Figs. 2d–f, it can be seen that  $TiO_2$  was aggregated on GR sheets in the  $TiO_2/2.0\%GR$  composite. It revealed that the  $TiO_2/GR$  composite was formed by grinding.

### 3.1.4. Diffuse reflectance spectroscopy

The UV-vis diffuse reflectance spectroscopy (DRS) was employed to investigate the optical properties of the  $TiO_2/GR$  composites. There was a typical strong absorption peak in the UV region less than 400 nm in Fig. 3, which was due to the transformation of electrons from the valence band (VB) of  $TiO_2$  to the conduction band (CB) [30]. Compared with the pure  $TiO_2$ , the absorption intensity of the composite significantly increased in the visible light region (400–800 nm), indicating the existence of C-doped  $TiO_2$  [30,32]. It was shown that the GR enhanced the visible-light absorption of  $TiO_2$  and was expected to improve the photocatalytic activity [33].

## 3.2. Adsorption and photocatalytic degradation of MB

### 3.2.1. Effect of pH

The pH can significantly influence on the catalytic properties of the  $TiO_2/GR$  composites. As shown in Fig. 4a, the MB removal rate gradually increased with increasing pH. When pH was 12, the degradation rate reached the maximum (98.18%). It was easier to degrade MB in alkaline conditions because a large number of hydroxyl ions adsorbed on the surface of the catalyst were captured by photogenerated holes to form a large number of hydroxyl radicals [34] which was an extremely strong non-selective oxidant during the photocatalytic reaction. Moreover, depending on the point of zero charge of  $TiO_2$  ( $pH_{pzc}$  6.5) [8,35], the  $TiO_2$  surface was positively charged at  $pH < pH_{pzc}$  and negatively charged at  $pH > pH_{pzc}$ . As a result, highly alkaline condition was favorable to the degradation of MB due to the columbic attraction between the positively charged  $TiO_2$  and MB which belongs to cationic dye. The following experiments were examined at pH 12.

### 3.2.2. Effect of catalyst dosage

The amount of catalyst is one of the important factors in the photocatalytic reaction. The degradation rate of MB increased with increasing the amount of  $TiO_2/2.0\%GR$  composite catalyst, as shown in Fig. 4b. However, when the amount of catalyst was more than 50 mg, the degradation rate

of MB tended to be stable. The number of available adsorption and catalytic sites on the catalyst surface increased with increasing in catalyst dosage, resulting in the observed enhancement in photocatalytic degradation efficiency. However, a further increase of the catalyst dosage did not increase the rate of photodegradation because of agglomeration of catalyst particles and light scattering and screening effect [8]. The optimal dosage of  $TiO_2/2.0\%GR$  for the removal of MB was found to be 50 mg, which was 2.5 g/L.

### 3.2.3. Content of graphene doped with $TiO_2$

It can be seen from Fig. 5 that under visible light irradiation, the photocatalytic activity of  $TiO_2$  was greatly improved from 72.89% to 98.18% by doping GR. Due to the characteristics of high carrier mobility ( $2 \times 10^5$  cm<sup>2</sup>/V s) [36], GR can rapidly migrate electrons into the lamellar structure of graphite, which effectively separated electrons and holes, thus improving the photocatalytic activity. In addition, the excited state energy of titanium dioxide in the  $TiO_2/GR$  composite, which was characterized by DRS, was reduced. Therefore, the visible light photocatalytic efficiency of  $TiO_2$  in  $TiO_2/GR$  composites was improved. However, excessive GR content would reduce the photo-trapping efficiency of the photocatalyst and lead to the decrease of the catalytic activity of the composite catalyst. The research suggested that the optimum wt.% of GR in  $TiO_2/GR$  composite was 2.0%.

### 3.2.4. Effect of initial MB concentration and kinetics of photocatalytic degradation

The effects of initial concentration of MB on photocatalytic degradation were studied from 0.0550 to 0.1350 mmol/L. It can be seen that the photocatalytic degradation efficiency of the  $TiO_2/GR$  composite decreased with an increase in the initial concentration of MB, as shown in Fig. 6a. It was due to block of the active sites of the catalyst and reduce the interaction of photons with these sites [8]. In addition, the degradation rate of MB increased until the reaction reached to the chemical equilibrium. The corresponding adsorption kinetics of MB on different time were shown in Fig. 6b, confirming the applicability of the pseudo-first-order kinetics with  $k_{app}$  from 0.0506 to 0.0144 1/min in the MB concentration range of 0.0550–0.1350 mmol/L. When the initial concentration of MB was 0.0550 mmol/L, the apparent rate constant of the  $TiO_2/2.0\%GR$  composite was 2.75 times than the one of pure  $TiO_2$ . It indicated that the  $TiO_2/2.0\%GR$  composite prepared by grinding possessed high catalytic activity. The apparent rate constant was calculated and presented in Table 2. It decreased as the initial MB concentration increased. Therefore, the optimum reaction time was 60 min under visible light irradiation, which was the same effect as reference reported in UV light [37].

### 3.2.5. Repetitive use of the catalyst

To investigate the repeatability of photo-catalyst activity, recycling experiments were carried out, which were completed under optimal conditions ( $TiO_2/2.0\%GR$  dosage 50 mg, pH = 12, irradiated by visible light 60 min). The

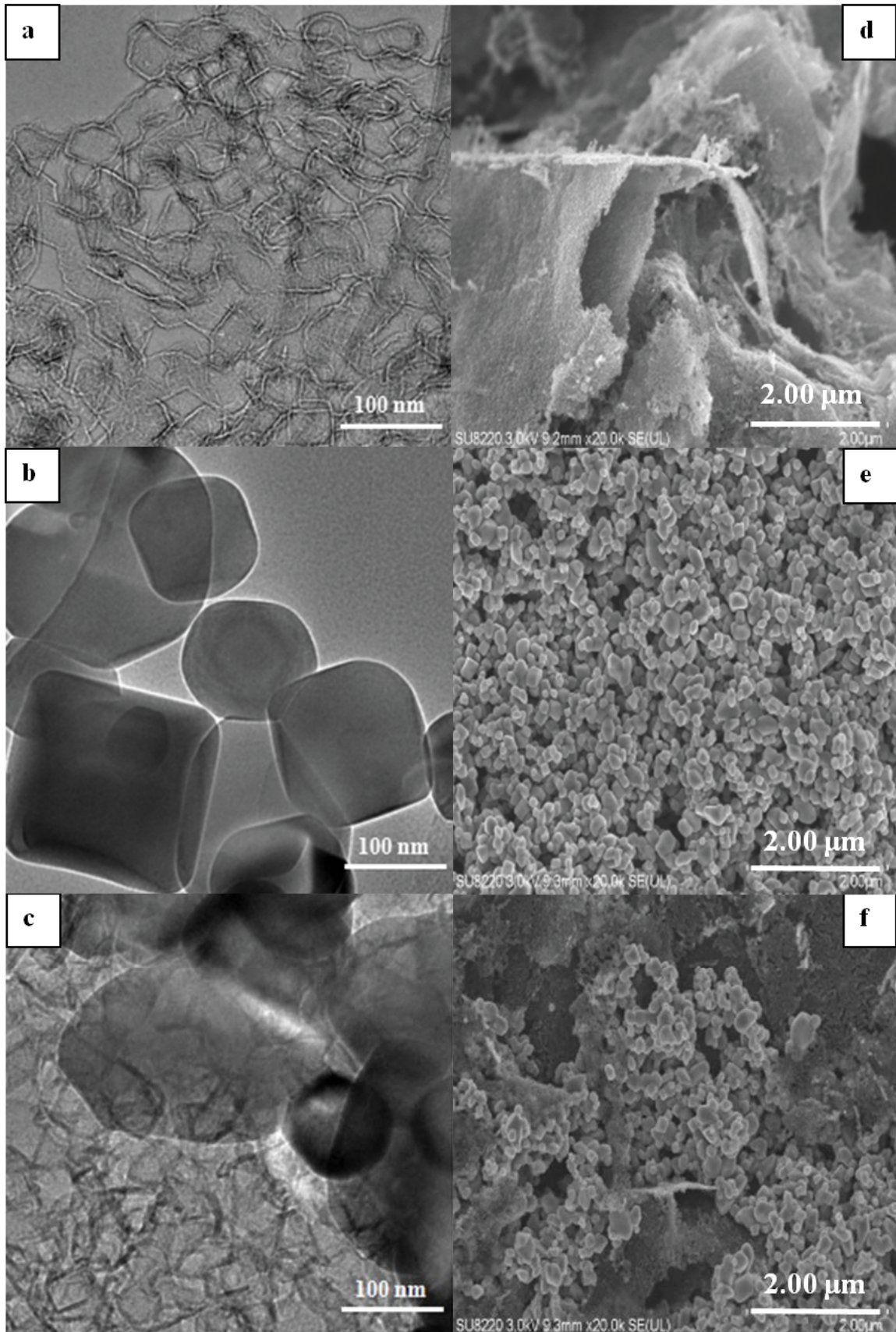


Fig. 2. TEM images of (a) GR, (b) TiO<sub>2</sub>, (c) TiO<sub>2</sub>/2.0% GR; SEM images of (d) GR, (e) TiO<sub>2</sub>, and (f) TiO<sub>2</sub>/2.0% GR.

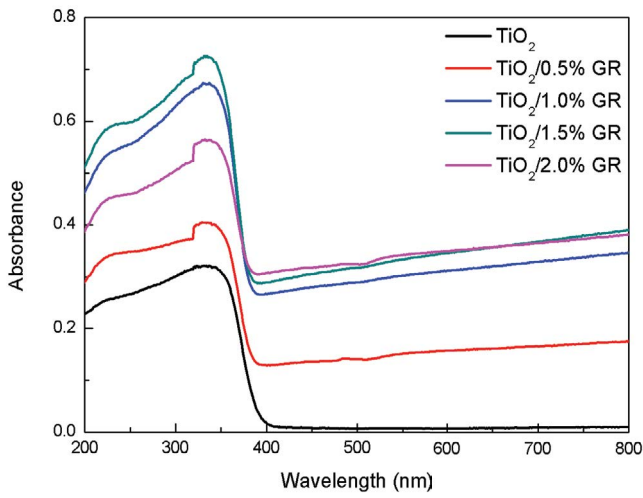


Fig. 3. UV-vis absorbance spectra of TiO<sub>2</sub> and TiO<sub>2</sub>/GR composites.

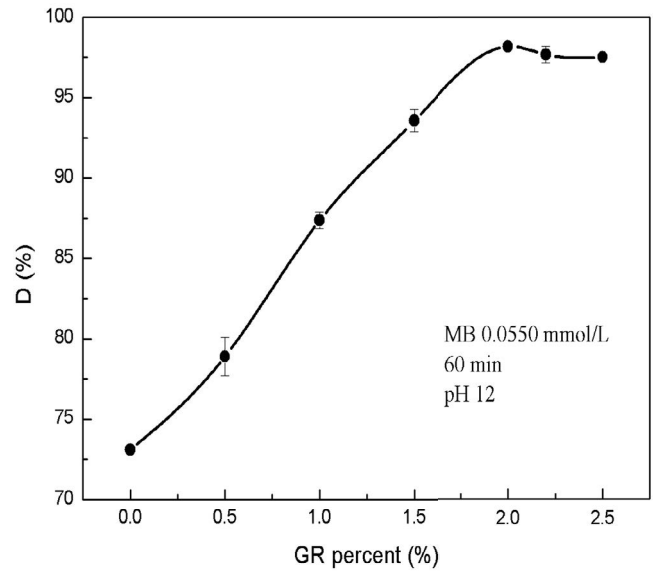


Fig. 5. Degradation rate of MB with different wt.% doped graphene.

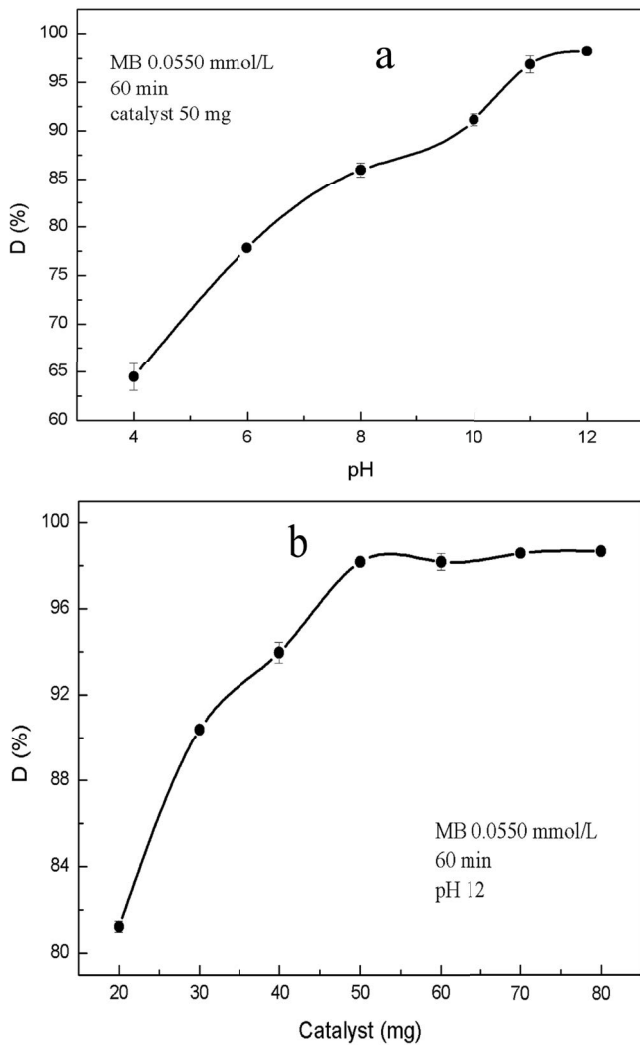


Fig. 4. Effect of (a) pH and (b) catalyst dosage on the degradation rate of MB.

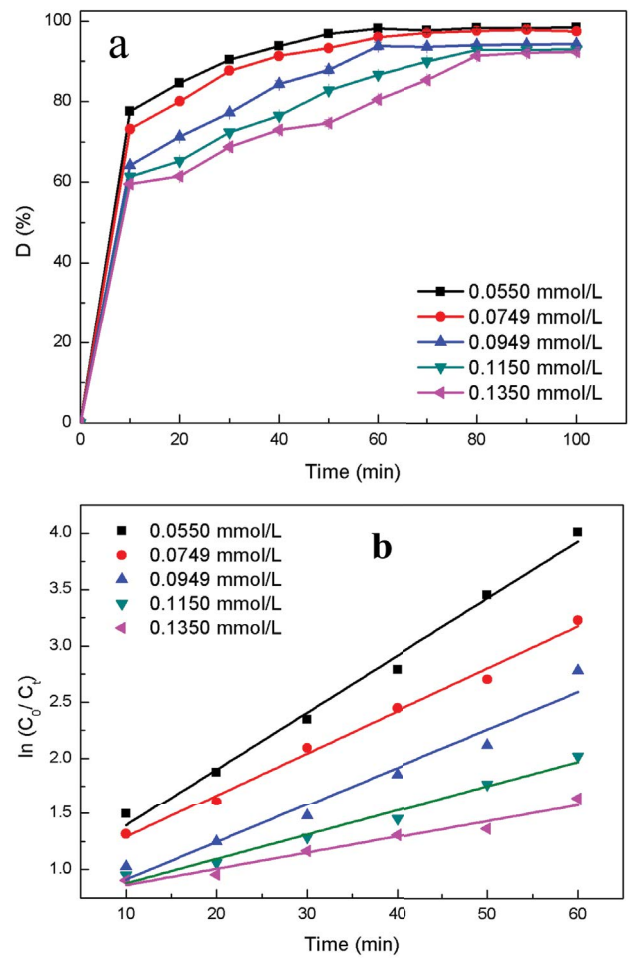


Fig. 6. Kinetics of MB photocatalytic degradation at different initial concentrations, (a) removal (%) vs. time, (b)  $\ln(C_0/C_t)$  vs. time (pH = 12).

Table 2  
Kinetic model parameters for the photodecomposition of MB

$c_0$ (mmol/L)	Pseudo-first-order kinetics	
	$k_a$	$R^2$
0.0550	0.0506	0.9902
0.0749	0.0376	0.9895
0.0949	0.0335	0.9489
0.1150	0.0216	0.9752
0.1350	0.0144	0.9583

results are shown in Fig. 7a. In comparison with the initial photo-degradation, the recovery efficiency of the  $\text{TiO}_2/2.0\%\text{GR}$  composite still exceeded 90% after the five cycles of the photo-degradation process. Although there was a slight decrease in the removal of MB (from 98.18% to 90.58%) after five cycles because the catalyst was contaminated by the generated by-products, the spent catalyst still possessed good photocatalytic activity. Hence, the  $\text{TiO}_2/2.0\%\text{GR}$  composite was a stable and reusable photo-catalyst for the effective removal of MB.

### 3.2.6. Photocatalytic performance under different lights irradiation

Considering the adsorption of  $\text{TiO}_2$  and graphene, the effects of three different light sources on the degradation rate were investigated, as shown in Fig. 7b. In the visible light, the  $\text{TiO}_2/2.0\%\text{GR}$  composite had the highest photocatalytic activity among  $\text{TiO}_2/2.0\%\text{GR}$  composite,  $\text{TiO}_2$ , and GR. It demonstrated that the catalytic performance of  $\text{TiO}_2$  was improved by doping GR into  $\text{TiO}_2$ . Meanwhile, the photocatalytic activity of  $\text{TiO}_2/2.0\%\text{GR}$  composite under the visible light was the same as that under UV light. It was indicated that the energy which was used to excite  $\text{TiO}_2$  in the composite was reduced, and the visible light absorption of  $\text{TiO}_2$  was enhanced which was consistent with the one by DR $\bar{\text{S}}$ . In the dark environment, both  $\text{TiO}_2$  and GR had a certain capability to remove MB because they can absorb the dye, resulting in a decrease of MB concentration.

### 3.2.7. Degradation of mixed dyes

There is usually more than one dye in the actual factory wastewater. Methyl orange (MO) is an anion dye. Methylene blue (MB) is a cationic dye. They were selected as the representative dye models. The degradation of the mixed dyes under different pHs was studied. The results are shown in Fig. 8a. The removal of MO decreased with increasing pH due to the columbic repulsion between the anion MO and negatively charged  $\text{TiO}_2/2.0\%\text{GR}$  at high pH. However, the degradation of MB in the mixed dyes increased with increasing pH, which was consistent with the above results (section 3.2.1 (Effect of pH)). The  $\text{TiO}_2/2.0\%\text{GR}$  composite can efficiently degrade anion dye MO under acidic conditions and cationic dye MB under alkaline conditions. Therefore, the separation of anion and cation dyes in the mixed system can be realized by changing pH. In addition, when  $\text{TiO}_2/2.0\%\text{GR}$  catalyzed the mixed dyes which

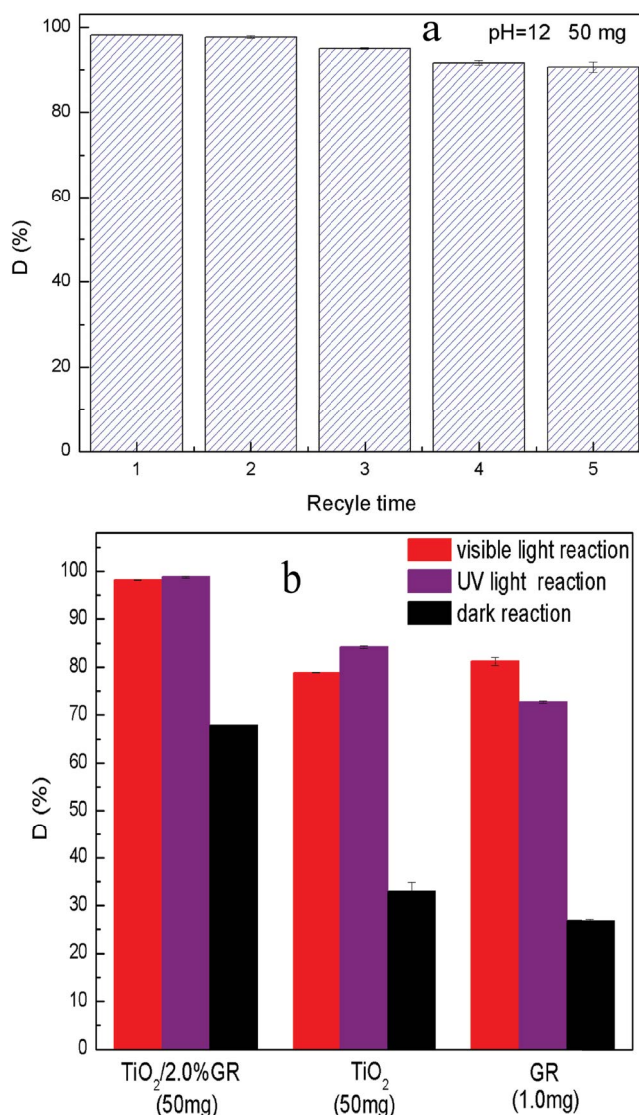


Fig. 7. (a) Results of recycling studies, (b) photodegradation rate of MB under UV light, visible light, and dark by  $\text{TiO}_2/2.0\%\text{GR}$ ,  $\text{TiO}_2$ , and GR catalysts, respectively.

consisted of MO and MB with a molar ratio of 1:1 without adjusting pH (pH 7.51), the degradation of the mixture was also outstanding, as shown in Fig. 8b. Based above,  $\text{TiO}_2/2.0\%\text{GR}$  composite had good degradation effects on both MO and MB and can be applied in practice.

### 3.3. Photocatalysis mechanism

A proposed mechanism is shown in Fig. 9. Similar photocatalytic degradation mechanism diagrams have been reported [13,30]. In short, the enhanced photocatalysis performance of  $\text{TiO}_2/\text{GR}$  can be attributed to the following three respects. Firstly, when the composite was exposed to the visible, the electrons ( $e^-$ ) on the valence band (VB) were excited and crossed the band gap into the conduction band (CB), resulting in an electron ( $e^-$ ) – hole ( $h^+$ ) pair [38].

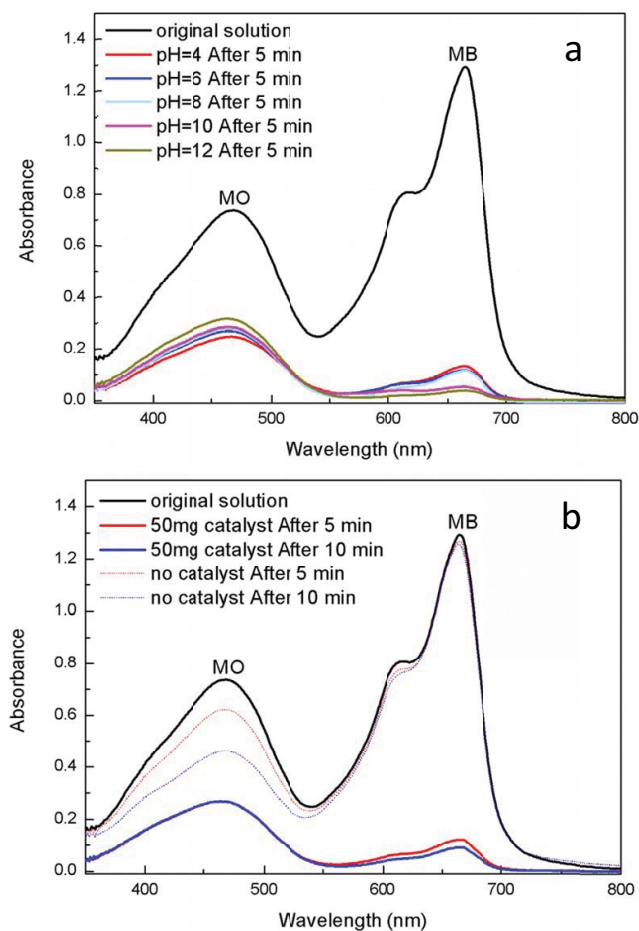


Fig. 8. (a) Effects of pH on the degradation of mixed dyes by  $\text{TiO}_2/2.0\% \text{GR}$ , (b) effects of time and  $\text{TiO}_2/2.0\% \text{GR}$  on the degradation of mixed dyes.

$\text{O}_2$  molecules which were adsorbed on the surface of  $\text{TiO}_2$  were very effective electron capture agents. Photoelectron ( $e^-$ ) reduced  $\text{O}_2$  to  $\cdot\text{O}_2^-$ .  $\text{H}_2\text{O}$  and  $\text{OH}^-$  adsorbed on the surface of  $\text{TiO}_2$  were oxidized to  $\cdot\text{OH}$  by  $\text{TiO}_2$  VB holes. These free radicals had a very high activity to catalyze the MB into non-toxic and harmless small molecules such as  $\text{NH}_4^+$ ,  $\text{SO}_4^{2-}$ ,  $\text{H}_2\text{O}$ ,  $\text{CO}_2$ , etc. [39]. Secondly, excited electrons can rapidly be migrated into GR lamellar structure by doping GR into  $\text{TiO}_2$  because of its high carrier mobility. This can effectively inhibit the recombination of photo-generated electron-hole pairs, produce more highly active free radicals, and promote the degradation of MB. Thirdly, GR had a unique two-dimensional plane structure of monatomic layer and a large number of  $\pi$  electrons, which can form  $\pi$ - $\pi$  bonds with pollutants containing square rings [40] and adsorb more pollutants. Thus, it can improve the photocatalytic degradation efficiency.

#### 4. Conclusion

The  $\text{TiO}_2/\text{GR}$  composites were synthesized easily by grinding which can be done in a large scale. Studies have shown that the composites possessed the structural and morphology characteristics of  $\text{TiO}_2$  and GR, respectively.

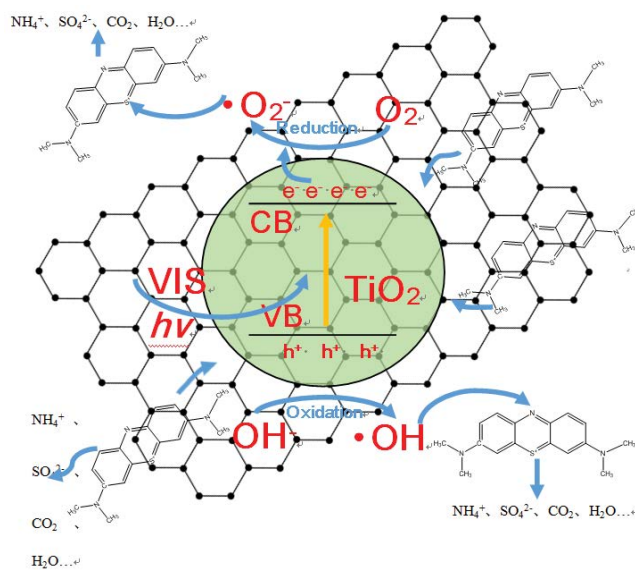


Fig. 9. Schematic mechanism for photocatalytic degradation of MB under visible light irradiation.

The catalytic efficiency of the  $\text{TiO}_2/2.0\% \text{GR}$  composite for degrading the MB reached 98.8% under visible light, which was much higher than one of pure  $\text{TiO}_2$ . It also possessed good stability by the anti-fatigue study. The kinetic study showed that the apparent rate constant of the  $\text{TiO}_2/2.0\% \text{GR}$  composite was 2.75 times than the one of pure  $\text{TiO}_2$ . In addition, the composite can selectively and rapidly degrade anion dye MO and cationic dye MB by adjusting pH. Therefore,  $\text{TiO}_2/2.0\% \text{GR}$  composite would be feasibly employed in dye wastewater treatment and have a great potential application in environmental pollution management.

#### References

- [1] J. Cheng, J. Chen, W. Lin, Y. Liu, Y. Kong, Improved visible light photocatalytic activity of fluorine and nitrogen co-doped  $\text{TiO}_2$  with tunable nanoparticle size, *Appl. Surf. Sci.*, 332 (2015) 573–580.
- [2] X.L. Shao, W. Lu, R. Zhang, F. Pan, Enhanced photocatalytic activity of  $\text{TiO}_2$ -C hybrid aerogels for methylene blue degradation, *Sci. Rep.*, 13 (2013) 3018:1–9, doi: 10.1038/srep03018.
- [3] R. Dagherir, P. Drogui, D. Robert, Modified  $\text{TiO}_2$  for environmental photocatalytic applications: a review, *Ind. Eng. Chem. Res.*, 52 (2013) 3581–3599.
- [4] Q. Gao, F. Fang, S. Zhang, Y. Fang, X. Chen, S. Yang, Hydrogenated F-doped  $\text{TiO}_2$  for photocatalytic hydrogen evolution and pollutant degradation, *Int. J. Hydrogen Energy*, 44 (2019) 8011–8019.
- [5] J. Yan, X. Li, F. Yang, X. Wang, W. Zhou, Y. Fang, S. Zhang, F. Peng, S. Zhang, Design and preparation of  $\text{CdS}/\text{H-3D-TiO}_2/\text{Pt}$ -wire photocatalysis system with enhanced visible-light driven  $\text{H}_2$  evolution, *Int. J. Hydrogen Energy*, 42 (2017) 928–937.
- [6] M.N. Chong, B. Jin, C.W.K. Chow, C. Saint, Recent developments in photocatalytic water treatment technology: a review, *Water Res.*, 44 (2010) 2997–3027.
- [7] N.R. Khalid, Z. Hong, E. Ahmed, Y. Zhang, H. Chan, M. Ahmad, Synergistic effects of Fe and graphene on photocatalytic activity enhancement of  $\text{TiO}_2$  under visible light, *Appl. Surf. Sci.*, 258 (2012) 5827–5834.
- [8] Z. Li, H. Wang, L. Zi, J. Zhang, Y. Zhang, Preparation and photocatalytic performance of magnetic  $\text{TiO}_2$ - $\text{Fe}_3\text{O}_4$ /graphene

- (RGO) composites under VIS-light irradiation, *Ceram. Int.*, 411 (2015) 634–643.
- [9] L. Deng, Y. Gu, W. Xu, Z. Ma, Synthesis of TiO<sub>2</sub>-graphene composite for using as a photocatalyst, *Chin. J. Appl. Chem.*, 29 (2012) 942–947.
- [10] L. Luo, X. Zhang, F. Ma, A. Zhang, L. Bian, X. Pan, F. Jiang, Photocatalytic degradation of bisphenol A by TiO<sub>2</sub>-reduced graphene oxide nanocomposites, *React. Kinet. Mech. Catal.*, 114 (2015) 311–322.
- [11] M. Green, J. Xu, H. Liu, J. Zhao, K. Li, L. Liu, H. Qin, Y. Zhu, D. Shen, X. Chen, Terahertz absorption of hydrogenated TiO<sub>2</sub> nanoparticles, *Mater. Today Phys.*, 4 (2018) 64–69.
- [12] W. Chen, Q. Lin, S. Cheng, M. Wu, Y. Tian, K. Ni, Y. Bai, H. Ma, Synthesis and adsorption properties of amphoteric adsorbent HA<sub>2</sub>/CMC-yAl, *Sep. Purif. Technol.*, 221(2019) 338–348.
- [13] C. Liu, L. Zhang, R. Liu, Z. Gao, X. Yang, Z. Tu, F. Yng, Z. Ye, L. Cui, C. Xu, Y. Li, Hydrothermal synthesis of N-doped TiO<sub>2</sub> nanowires and N-doped graphene heterostructures with enhanced photocatalytic properties, *J. Alloys Compd.*, 656 (2016) 24–32.
- [14] J. Li, D. Luo, C. Yang, S. He, S. Chen, J. Lin, L. Zhu, X. Li, Copper(II) imidazole frameworks as highly efficient photocatalysts for reduction of CO<sub>2</sub> into methanol under visible light irradiation, *J. Solid State Chem.*, 203 (2013) 154–159.
- [15] L. Li, J. Xu, G. Li, X. Jia, Y. Li, F. Yang, L. Zhang, C. Xu, J. Gao, Y. Liu, Z. Fang, Preparation of graphene nanosheets by shear-assisted supercritical CO<sub>2</sub> exfoliation, *Chem. Eng. J.*, 284 (2016) 78–84.
- [16] H. Feng, R. Cheng, X. Zhao, X. Duan, J. Li, A low-temperature method to produce highly reduced graphene oxide, *Nat. Commun.*, 4 (2013) 1539–1546.
- [17] Q. Xu, J. Yu, J. Zhang, J. Zhang, G. Liu, Cubic anatase TiO<sub>2</sub> nanocrystals with enhanced photocatalytic CO<sub>2</sub> reduction activity, *Chem. Commun.*, 51 (2015) 7950–7953.
- [18] Y. Zhang, Z. Zhao, J. Chen, L. Cheng, J. Chang, W. Sheng, C. Hu, S. Cao, C-doped hollow TiO<sub>2</sub> spheres: *in situ* synthesis, controlled shell thickness, and superior visible-light photocatalytic activity, *Appl. Catal., B*, 165 (2015) 715–722.
- [19] T. Lavanya, K. Sathesh, M. Dutta, N.V. Jaya, N. Fukata, Superior photocatalytic performance of reduced graphene oxide wrapped electrospun anatase mesoporous TiO<sub>2</sub> nanofiber, *J. Alloys Compd.*, 615 (2014) 643–650.
- [20] J. Yang, S. Mei, J.M.F. Ferreira, Hydrothermal synthesis of nanosized titania powders: influence of peptization and peptizing agents on the crystalline phases and phase transitions, *J. Am. Ceram. Soc.*, 83 (2000) 1361–1368.
- [21] P. Zhang, C. Shao, Z. Zhang, M. Zhang, J. Mu, Z. Guo, Y. Liu, TiO<sub>2</sub>@carbon core/shell nanofibers: controllable preparation and enhanced visible photocatalytic properties, *Nanoscale*, 3 (2011) 2943–2949.
- [22] R. Zukerman, L. Vradman, L. Titelman, L. Zeiri, N. Perkas, A. Gedanken, M.V. Landau, M. Herskowitz, Effect of SBA-15 microporosity on the inserted TiO<sub>2</sub> crystal size determined by Raman spectroscopy, *Mater. Chem. Phys.*, 122 (2010) 53–59.
- [23] A. Ferrari, J. Meyer, V. Scardaci, C. Casiraghi, M. Lazzeri, F. Mauri, S. Piscanec, D. Jiang, K. Novoselov, S. Roth, A. Geim, Raman spectrum of graphene layers, *Phys. Rev. Lett.*, 97 (2006), doi: 10.1103/PhysRevLett.97.187401.
- [24] P. Dubey, P. Tripathi, R. Tiwari, A. Sinha, O. Srivastava, Synthesis of reduced graphene oxide–TiO<sub>2</sub> nanoparticle composite systems and its application in hydrogen production, *Int. J. Hydrogen Energy*, 39 (2014) 16282–16292.
- [25] J. Huang, Q. Tang, W. Liao, G. Wang, W. Wei, C. Li, Green preparation of expandable graphite and its application in flame-resistance polymer elastomer, *Ind. Eng. Chem. Res.*, 56 (2017) 5253–5261.
- [26] S. Lin, C. Shih, M. Strano, B. Daniel, Molecular insights into the surface morphology, layering structure, and aggregation kinetics of surfactant-stabilized graphene dispersions, *J. Am. Chem. Soc.*, 133 (2011) 12810–12823.
- [27] L. Malard, M. Pimenta, G. Dresselhaus, M.S. Dresselhaus, Raman spectroscopy in graphene, *Phys. Rep.*, 473 (2009) 51–87.
- [28] T. Peng, B. Liu, X. Gao, L. Luo, H. Sun, Preparation, quantitative surface analysis, intercalation characteristics and industrial implications of low temperature expandable graphite, *Appl. Surf. Sci.*, 444 (2018) 800–810.
- [29] E. Vahidzadeh, S. Fatemi, A. Nouralishahi, Synthesis of a nitrogen-doped titanium dioxide-reduced graphene oxide nanocomposite for photocatalysis under visible light irradiation, *Particuology*, 41 (2018) 48–57.
- [30] F. Wu, W. Liu, J. Qiu, J. Li, W. Zhou, Y. Fang, S. Zhang, Enhanced photocatalytic degradation and adsorption of methylene blue via TiO<sub>2</sub> nanocrystals supported on graphene-like bamboo charcoa, *Appl. Surf. Sci.*, 358 (2015) 425–435.
- [31] Q. Dong, G. Wang, B. Qian, C. Hu, Y. Wang, J. Qiu, Electrospun composites made of reduced graphene oxide and activated carbon nanofibers for capacitive deionization, *Electrochim. Acta*, 137 (2014) 388–394.
- [32] A. Xu, Y. Gao, H. Liu, The preparation, characterization, and their photocatalytic activities of rare-earth-doped TiO<sub>2</sub> nanoparticles, *J. Catal.*, 207 (2002) 151–157.
- [33] H. Zhang, X. Lv, Y. Li, Y. Wang, J. Li, P25-graphene composite as a high performance photocatalyst, *ACS Nano*, 4 (2010) 380–386.
- [34] A. Nedoloujko, J. Kiwi, TiO<sub>2</sub> speciation precluding mineralization of 4-tert-butylpyridine accelerated mineralization via Fenton photo-assisted reaction, *Water Res.*, 34 (2000) 3277–3284.
- [35] A.G. Rincón, C. Pulgarin, Effect of pH, inorganic ions matter and H<sub>2</sub>O<sub>2</sub> on *E. coli* K12 photocatalytic inactivation by TiO<sub>2</sub> implications in solar water disinfection, *Appl. Catal., B*, 51 (2004) 283–302.
- [36] Y. Zhang, Y. Tan, H. Stormer, K. Philip, Experimental observation of the quantum Hall effect and Berry's phase in graphene, *Nature*, 438 (2005) 201–204.
- [37] Q. Mao, D. Liu, G. Li, Q. Wang, C. Xue, Y. Bai, TiO<sub>2</sub>/SGNs as photocatalyst for degradation of water pollutants, *Desal. Water Treat.*, 161 (2019) 171–180.
- [38] P.M. Martins, V. Gomez, A.C. Lopes, C.J. Tavares, G. Botelho, S. Irueta, Improving photocatalytic performance and recyclability by development of Er-doped and Er/Pr-codoped TiO<sub>2</sub>/poly(vinylidene difluoride)-trifluoroethylene composite membranes, *J. Phys. Chem. C*, 118 (2014) 27944–27953.
- [39] N. Bell, Y. Ng, A. Du, H. Coster, S. Smith, R. Amal, Understanding the enhancement in photoelectrochemical properties of photocatalytically prepared TiO<sub>2</sub>-reduced graphene oxide composite, *J. Phys. Chem. C*, 115 (2011) 6004–6009.
- [40] M. Allen, V. Tung, R. Kaner, Honeycomb carbon: a review of graphene, *Chem. Rev.*, 110 (2009) 132–145.